Zinc and cadmium mapping by NanoSIMS within the root apex after short-term exposure to metal contamination

Gabrijel Ondrasek[1,2*], Zed Rengel[1], Peta L. Clode[3], Matt R. Kilburn[3], Paul Guagliardo[3], Davor Romic[2]

[1]UWA School of Agriculture and Environment, The University of Western Australia, 35 Stirling Highway, Perth WA 6009, Australia

[2]Faculty of Agriculture, The University of Zagreb, Svetosimunska cesta 25, 10 000 Zagreb, Croatia, European Union

[3]The Centre for Microscopy, Characterisation and Analysis, The University of Western Australia, 35 Stirling Highway, Crawley WA 6009, Australia

*Correspondence:

Gabrijel Ondrasek

gondrasek@agr.hr

Keywords: ICP-MS, High-resolution secondary ion mass spectrometry, ^{70}Zn, Cd, Root apex, Radish

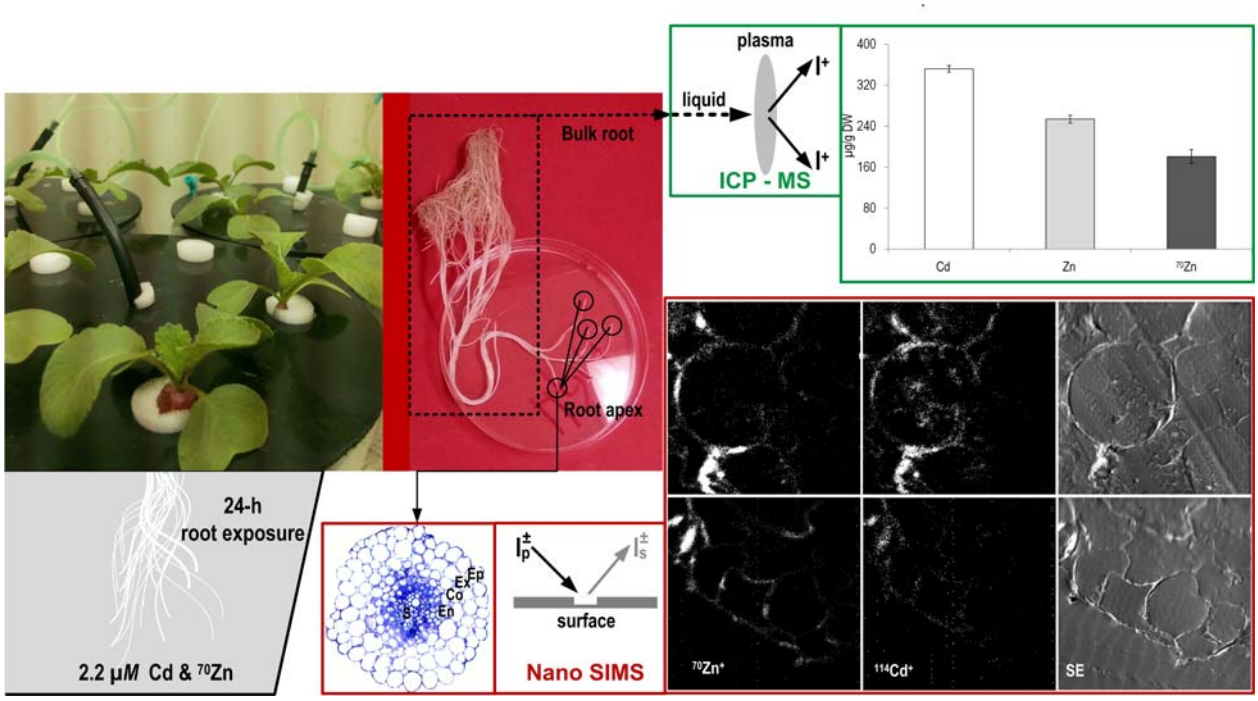

Graphical abstract

Abstract

Zinc as a micronutrient and cadmium as a nonessential toxic element share similar pathways for entering plant tissues and thus may be antagonistic. In nutrient solution culture, 17-day-old radish (*Raphanus sativus* L) plants were exposed to short-term (24 h) equimolar metal contamination (2.2 µ*M* of each ^{70}Zn and total Cd) to investigate the *in situ* Zn/Cd distribution in the apical root tissues using high-resolution secondary ion mass spectrometry (NanoSIMS) imaging. Inductively-coupled plasma mass spectrometry analysis of bulk root tissue confirmed large root uptake of both metal elements. After 24-hour exposure the total root concentration (in µg/g DW) of ^{70}Zn was 180±24 (mean±SE) and of total Cd 352±11. NanoSIMS mapping was performed on the cross sections of the radish root apex as a crucial component in root growth and uptake of water and nutrients from soil. Elemental maps of ^{70}Zn and ^{114}Cd isotopes revealed greater enrichment of both metals in the outer epidermal root layer than in cortical tissues and especially stele, confirming the epidermal root cells as preferential sites of metal uptake, and indicating relatively slow and less-intensive metal transport into other parts (edible hypocotyl, shoot) of metal-

sensitive radish. NanoSIMS has been confirmed as a powerful tool for spatial detection and visualisation of some ultra-trace metal isotopes (e.g. ^{70}Zn) in the fast-growing root tips. However, precise (sub)cellular mapping of diffusible metallic ions (Cd, Zn) remains a technically-challenging task in plant specimens given an unavoidable compromise between optimising methodology for structural preservation vs. authentic *in vivo* ion localisation.

INTRODUCTION

Biosphere contamination by trace metal elements is one of the most critical environmental and sustainability problems in the 21st century. Among numerous trace metals, cadmium (Cd) and its hydro-biogeochemical interactions in the terrestrial rhizosphere (e.g. Adriano et al., 2004; Wang et al., 2012) or marine and fresh water ecology (Rehkämper et al., 2011) are widely reported, including its routes to the human food chain (Huang et al., 2017; Sigel et al., 2013). The most important highlights are: i) rhizosphere biogeochemistry of Cd is highly pH-dependent; ii) availability of Cd, especially in environments with relatively low pH (<6.0), increases; iii) Cd has a high potential for the complexation and chemisorption reactions with a range of potentially available in/organics (e.g. simple inorganic salts, high-/low-molecular-weight organic ligands); iv) its essential biological function in plants is still unconfirmed, although it shares the uptake/translocation/deposition pathways with some essential major/trace nutrients; v) Cd phytoaccumulation in most cultivated species dominantly takes place within the tissue where primary nutrient uptake occurs (roots, tubers, hypocotyls); vi) Cd phytoaccumulation represents the main entry route into the human/animal diet; and vii) Cd is toxic to a wide range of organisms, including plants and humans, and is potentially carcinogenic, with no obvious safe threshold limit (Ondrasek 2013 and references therein).

Over the last several decades, special attention was paid to food security and producing food free of metal contamination. In that respect, understanding the interactions of Cd with certain essential phyto-nutrients is particularly important. Namely, due to physical and chemical similarities (e.g. ionic radii, redox activity, Lewis acidity) between Cd and some divalent metal phyto-nutrients (e.g. Zn, Mn, Fe), non-essential Cd would most likely enter the plant system via routes specific for the similar essential elements (e.g. Li et al., 2012). For instance, Cd uptake across the root cell plasma membrane was shown to occur via a concentration-dependent mechanism exhibiting saturable kinetics (Hart et al., 1998; Salt et al., 1995), with confirmed Cd-Zn, Cd-Mn and Cd-Cu competition (Hart et al., 2002; Salt et al., 1995) or Cd-Fe complementarity (Nakanishi et al., 2006). Also, the severity of Cd phyto-toxicity was shown to be modified by some essential elements such as Zn, Ca, Fe, Cu and Mn (Das et al., 1997). Zinc as an essential trace metal phyto-nutrient might be of crucial importance (e.g. Rengel, 2015), given that Zn is the second most abundant transition metal in organisms (after Fe), and the only metal represented in all six enzyme classes (Broadley et al., 2007), i.e. essential for activity of more than 300 enzymes (Li et al., 2012).

Zn and Cd are common constitutes of (i) the ores that are used as raw materials for inorganic fertilisers, and (ii) some other soil amendments (limestone, sewage sludge, biosolids), i.e. the main anthropogenic trace metal inputs in the majority of agro-ecosystems (Rengel, 2015; Savic et al., 2015). As some of the most mobile and phyto-available trace metals in the rhizosphere, and due to relatively low selectivity of relevant transmembrane ion transporters, Zn and Cd relatively easily cross the soil-root interface (e.g. Clemens, 2006; Pearson and Rengel, 1995). Finally, the fact that Cd is a phytotoxic (Wang et al., 2012) and Zn an essential (Buffet et al. 2012; Li et al., 2012) metal element makes their interaction vital as it raises the possibility that the harmful effects of Cd might be minimised and/or prevented by Zn (Das et al., 1997; Ondrasek et al., 2012). However, although Zn is a micronutrient, it also can induce toxicity to plants

(Rengel, 2015) and other organisms (Pérez-López et al., 2008) depending on the concentration and the duration of exposure.

A crucial tool in plant nutrition studies is the visualization of element distributions at different scales, from the tissue to the (sub)cellular levels, given that spatial information provides important clues to understanding the mechanisms of regulation of the homeostasis of essential and toxic metals (Moore et al., 2014). Secondary Ion Mass Spectrometry (SIMS) imaging techniques are an increasingly valuable tool in many areas of biological sciences used for *in situ* isotopic analysis at a subcellular scale (Chandra, 2008; Tartivel et al., 2012). SIMS analysis allows *in situ* bio imaging of different (non)diffusible elements and isotopes (e.g. ^{13}C, ^{26}Mg, ^{41}K, ^{44}Ca, ^{81}Br, ^{195}Pt) and molecules (e.g. $H_2{}^{18}O$, D_2O, etc.) by scanning a specimen with a high-energy primary ion beam to sputter atoms, molecules and electrons from the sample surface (Cennerazzo et al., 2017; Eybe et al., 2013; 2009; Kilburn et al., 2010; Metzner et al., 2010; Tartivel et al., 2012). In a dynamic SIMS approach, reactive primary ion beams (Cs^+, O^-) are used to enhance secondary ion yields of the elements of interest (Boxer et al., 2009). Ionized species (secondary ions) are then separated on the basis of their mass-to-charge ratio using a high-performance mass spectrometer, and are correlated with their spatial origin to form a chemical map (Smart et al., 2010). Unfortunately, Zn and Cd have relatively low secondary ion yields generated after bombardment by the O^- or Cs^+ primary beam (up to several orders of magnitude lower than some other elements such as Si, Al or Mg). Hence, obtaining clear Zn and Cd signals at trace levels from biological specimens by NanoSIMS is expected to be challenging.

So far, most studies of *in situ* mapping and prediction of Cd and/or Zn in plant tissues (e.g. high-resolution secondary ion mass spectrometry SIMS, synchrotron X-ray fluorescence S-XRF, scanning electron microscopy with energy-dispersive X-ray SEM-EDX, scanning transmission electron microscopy STEM, proton-induced X-ray emission PIXE, laser ablation inductively-coupled plasma mass spectroscopy LA-ICP-MS, combination of scanning ion-selective electrode technique SIET and/or micro electrode ion flux measurement MIFE with fluorescence

109 microscopy) are based on relatively long-term (several weeks/months) exposure and/or exposure
110 to contamination-relevant concentrations (>10 μ*M*) using metal-(hyper)tolerant plant species
111 (metalophytes) or salt-tolerant (halophytes) (e.g. Lu et al., 2008; Lombi et al., 2011; Li et al.,
112 2012; Moore et al., 2014; Villafort Carvalho et al., 2015). Metallophytes (e.g. *Arabidopsis halleri, Noccaea caerulescens*) have been widely studied in phytoremediation, given their high metal
113
114 tolerance and an extremely high potential of root-to-shoot metal transfer and metal accumulation
115 in aerial tissues (e.g. Lu et al., 2008). In contrast, elucidation of (sub)cellular metal distribution in
116 non-metalophyte species might be markedly more challenging because of substantially lower
117 concentration of metallic isotopes of interest; this challenge has been addressed in the present
118 study.
119 The main objective was to examine the *in situ* Zn and Cd distribution in the root apices of
120 metal-sensitive radish (*Raphanus sativus*) plants after short-term (24 h) exposure to low
121 concentration (2.2 μ*M*) of each Cd and Zn using high-resolution secondary ion mass spectrometry
122 (NanoSIMS).
123
124 **MATERIALS AND METHODS**
125
126 **Plant growth conditions**
127 Radish (*Raphanus sativus* L. cv. Cherry Belle) was hydroponically grown in a fully-
128 controlled growth chamber (12/12 light/dark period, air temperature 22/17°C, air humidity
129 60/80%, and 350 μmol m^{-2} s^{-1} photosynthetically active radiation supplied by high pressure metal-
130 halide lamps) at the University of Western Australia (Perth, Australia). In brief, uniform seeds of
131 radish were surface-sterilized by soaking in 70% (v/v) ethanol for 1 min followed by 1% (v/v)
132 sodium hypochlorite for 5 min, and were then pre-germinated in ultrapure deionized water (18
133 mΩ cm^{-1}) obtained from a Milli-Q system (Millipore Corp, Milford, CT, USA) for 48 h.
134 Ultrapure water was used for the preparation of all other nutrient and stock solutions from lab-

grade chemicals. Six uniform germinated seeds were transferred to a floating plastic net in 4-L non-transparent plastic pots filled with nutrient solution of the following composition: $Ca(NO_3)_2$ 2.5 m*M*, KNO_3 2.5 m*M*, KH_2PO_4 0.5 m*M*, $MgSO_4$ 1.0 m*M*, MES 1 m*M* (at pH 6.0), $FeSO_4$ 50 µ*M*, H_3BO_3 5.0 µ*M*, $MnCl_2$ 3.70 µ*M*, $ZnSO_4$ 0.64 µ*M*, $CuSO_4$ 0.52 µ*M*, $NiSO_4$ 0.1 µ*M* and Na_2MoO_4 0.02 µ*M*. After 6 days, three uniform seedlings, supported by 2-cm-long and 1-cm-wide poly-foam were positioned in holes cut into tight-fitting lids of 4-L pots filled with nutrient solution (containing double the nutrient concentrations listed above) (Figure 1a).

All nutrient solutions were continuously aerated and changed every 3 days. On 17th day after germination, plant roots were exposed to equimolar (2.2 µ*M*) metal contamination of ^{70}Zn (as zinc sulphate heptahydrate with 95.42% of ^{70}Zn-enrichment, Trace Sciences International Corp., Ontario, Canada) and Cd (as cadmium nitrate tetrahydrate with all naturally-occurring isotopes, Ajax Chemicals Ltd., Sydney, Australia) in the nutrient solution for 24 hours in triplicate. Before applying the ^{70}Zn/Cd treatment, roots were placed in ultrapure water for 5 min, followed by 5 m*M* $CaCl_2$ for 10 min (to improve desorption of adsorbed Zn and potential inadvertent Cd contamination, if any) and then ultrapure water for 15 min. After 24-hour exposure to the ^{70}Zn/Cd treatment, roots were rinsed repeatedly in ultrapure water in preparation for sampling.

Sampling and sample preparation for the NanoSIMS

For the NanoSIMS analyses, several apical root sections (approximately up to 5 mm in length) in each of the three replicates were excised by a razor (Figure 1a) and immediately plunged into liquid nitrogen slush to immobilize and preserve the elements of interest. At least four independent root sections (from each tested plant) were then stored in liquid N until the process of freeze substitution. Freeze substitution of root apices was done in an anhydrous mixture of 10% v/v acrolein (fixative to preserve cells) in diethyl ether (solvent) over 24 days

using a fully-controlled freeze-substitution system Reichert AFS (Leica) according to the procedures explained in detail elsewhere (Kilburn and Clode, 2014). Unlike substitution in acetone, this method is known to preserve diffusible ions for subsequent cellular analysis. After 24 days of substitution, samples were brought to room temperature, and root apices were washed in anhydrous ether three times (20 min each time). Then, root apices were embedded gradually in Araldite 502 resin, using a graded resin-ether (v/v) mixtures: 10%, 25%, 50%, 75% and 100% for 2 h each followed by 100% resin overnight. Over the next 4 days, the samples were kept in 100% Araldite 502 resin that was changed twice a day. Finally, individual root apices were placed into moulds filled with resin and polymerized at 60°C for 24 h under the vacuum.

One-µm-thick sections of the resin-embedded root apices were cut on a glass knife using an ultramicrotome (Leica). Sections were then transferred on a very small droplet of Milli-Q water onto glass slide and stained with 0.2% (v/v) toluidine blue to observe the root structure. Given that the root structures should not have changed significantly at a short distance (thickness) between adjoining sections (e.g. Moore et al., 2014), immediately after the glass slide section of the root apex, new 1-µm-thick sections were cut and placed onto 7 mm x 7 mm silicon wafers for NanoSIMS analysis. To prevent charging during the NanoSIMS analysis, the samples were coated with a 10 nm layer of gold before loading into a NanoSIMS vacuum chamber.

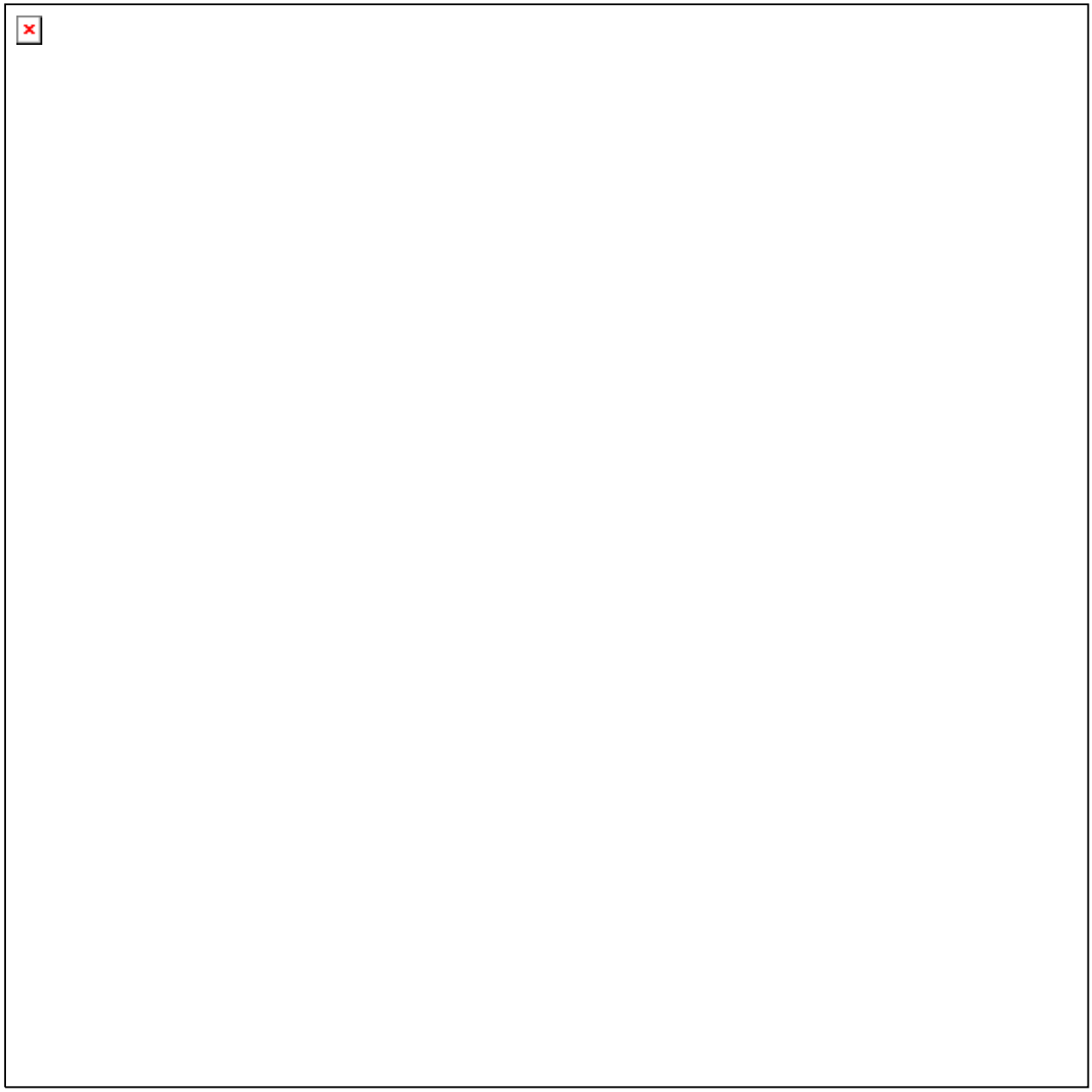

Figure 1. (a) An 18-d-old test plant after 24-hour root medium exposure to the equimolar (2.2 μ*M*) ^{70}Zn/Cd treatment, and (b) a root apex just before sampling. Scale bars: 20 mm.

(c) Optical micrograph of resin-embedded cross section of the radish apical root tissue prepared by freezing in liquid N slush followed by freeze substitution, showing well preserved morphological cell structures: epidermis (Ep), cortex (Co), endodermis (En), stele (S) and xylem vessels (asterisks). Scale bar: 50 μm.

(d) Schematic presentation of cross section of the root apex with the principal water/element pathways: apoplastic via the cell walls/intercellular spaces (dotted line), symplastic via the

cytoplasm/plasmodesmata (grey line) and transcellular, in and out of cells via the plasma membrane/apoplast (black line) (according to Bramley et al., 2009; Ma and Yamaji, 2008).

(e) Mosaic picture composed of the reflectance optical micrographs of serial cross sections of a radish apical root tissue (1, 2, 3) and 0.1 mL of dehydrated standard solution of ^{70}Zn serving as a reference standard material (Std), all prepared on the silicon wafers (7 mm x 7 mm) before coating with a 10 nm layer of gold and placing into a NanoSIMS vacuum chamber. Scale bar: 100 µm.

Sampling and sample preparation for ICP-MS

The remaining root tissue (after sampling for NanoSIMS) from each replicate was dried at 70°C for 48 h. Dried root samples were digested in a mixture of concentrated nitric (HNO_3) and perchloric acid ($HClO_4$) according to the procedure explained in detail by Ondrasek et al. (2018). In short, the total amount of root sample was weighed and digested in 5 mL of concentrated HNO_3 at 95-100 °C for ~45 min, until all particulate material was dissolved. The digests were allowed to cool down and were supplemented with 0.5 mL of concentrated $HClO_4$ and were heated to 145-150 °C for ~30 min. After cooling, the digests were transferred with three rinses by ultrapure water to 10 mL vials containing 5 µg of yttrium serving as an internal standard (i.e. to account for an instrument drift and sensitivity; e.g. Buffet et al., 2012) and stored for further analyses. In each analytical batch, at least three reagent blanks (i.e. ultrapure water) and one internationally certified reference plant material (WEPAL, Wageningen, The Netherlands) were included. Importantly, the measurements of all reference standard samples and blanks yielded results that were within declared values (i.e. <2%). The total (bulk) concentration of ^{70}Zn and Cd in digested root extracts was determined using inductively-coupled plasma mass spectroscopy (ICP-MS) (Agilent Technologies 7700x, Santa Clara, CA, USA).

212

213 **NanoSIMS analyses**

214 All high-resolution maps were acquired using a NanoSIMS 50 (Cameca, France)
215 instrument at the University of Western Australia. The NanoSIMS 50 is a dynamic SIMS that
216 allows parallel collection of up to five ion species with both high mass and high spatial resolution
217 (Smart et al., 2007). The NanoSIMS incorporates an ion source, i.e. microprobe comprising
218 reactive ions of caesium (with a diameter of ~50 nm) and oxygen (with a diameter of ~200 nm),
219 coupled to a specially designed magnetic sector mass analyser to achieve maximum instrumental
220 sensitivity and to ensure comparatively low current primary ion beams to limit sample
221 destruction, allowing the use of 1-µm-thin sample sections (Clode et al., 2007) as were prepared
222 in this study. A primary ion beam (Cs^+ or O^-) was scanned across the surface of specimens
223 prepared as explained above, and the sputtered secondary ions were extracted to a double-
224 focusing mass spectrometer ensuring the sub-100 nm lateral resolution whilst imaging negatively
225 charged secondary ions, and sub-300 nm lateral resolution for positive secondary ions (Moore et
226 al., 2011).

227 In this study apical root sections were examined by using Cs^+ and O^- primary ion beams
228 separately. Firstly, positive secondary ions were sputtered using an O^- primary beam, with a beam
229 current of 30 pA and an impact energy of approximately 16 keV rastered over an area of
230 approximately 50 µm x 50 µm. The positive secondary ions $^{64}Zn^+$, $^{70}Zn^+$ and $^{114}Cd^+$ were
231 recorded simultaneously. The instrument was tuned to high mass resolution (6,000 mass resolving
232 power) to minimize/exclude isobaric interferences. Ion images were acquired at a resolution of
233 256 x 256 pixels with count times of 100 ms per pixel, taking about 3 h per image. All areas were
234 pre-sputtered with the primary ion beam prior to acquisition to remove surface contamination and
235 to enhance the generation of secondary ions.

To acquire additional information about the intracellular root structure (containing C, N, S), negative secondary ions $^{16}O^-$, $^{12}C^-$, $^{26}CN^-$, $^{32}S^-$ and $^{35}Cl^-$ were sputtered over the same root cell area using a Cs^+ primary beam with a beam current of 10 pA and an impact energy of approximately 16 keV. Additionally, the ion maps were collected simultaneously with the secondary electron (SE) maps generated by the ion beam. Secondary electrons are produced during the sputtering process, and these can be used to improve visualisation of both sample morphology and surface topography (Moore et al., 2011).

Images showing $^{70}Zn/^{64}Zn$ ratios were obtained by normalizing the ^{70}Zn counts to the ^{64}Zn counts for each pixel in the ion images. The numerical $^{70}Zn/^{64}Zn$ ratio data were extracted directly from the $^{70}Zn/^{64}Zn$ ion images by selecting the regions of interest and the pixels defining certain structural features on the normalized image using the Open MIMS plugin for ImageJ (http://www.nrims.hms.harvard.edu/NRIMS_ImageJ.php, Harvard, Cambridge, MA, USA).

RESULTS AND DISCUSSION

Bulk concentration of metals of interest determined by ICP-MS

ICP-MS is one of the most advanced routine techniques for detection of metallic isotope concentrations with high sensitivity (from mg/kg to below µg/kg) and simple spectra in various biological specimens (Caruso and Montes-Bayon, 2003). Therefore, elemental (isotopic) detection by ICP-MS is commonly used in (pre)screening prior to isotopic mapping by NanoSIMS (e.g. Moore et al., 2011; Moore et al., 2014), given restricted sensitivity of SIMS analysis (around mg/kg in appropriate sample/analyte combinations) (Moore et al., 2010) because of a specific MS detector in NanoSIMS 50 Cameca we had access to. The elemental bulk concentrations obtained by ICP-MS provide generic information regarding the feasibility of SIMS analyses in determining distribution patterns (i.e. local element concentration) (e.g. Moore et al., 2012).

Naturally-occurring Zn comprises five stable isotopes (^{64}Zn, ^{66}Zn, ^{67}Zn, ^{68}Zn and ^{70}Zn), with ^{64}Zn and ^{68}Zn being the most abundant (49 and 19%, respectively) and ^{70}Zn the least abundant (0.6%), confirming its ultra-rare isotopic presence. Among naturally-occurring Cd stable (or quasi stable) isotopes, the most abundant are ^{112}Cd and ^{114}Cd (29 and 24%, respectively). At the onset of the 24-h metal treatment in the study presented here, radish roots were exposed to ^{70}Zn and the natural isotope mixture of Cd; these metal isotopes were taken up and accumulated in roots in relatively high concentrations (Figure 2) as confirmed by the ICP-MS analyses of the total (bulk) root samples. We used isotopically labelled ^{70}Zn in the 24-h treatment to compare its pattern of distribution with the most abundant isotope ^{64}Zn (e.g. Buffet et al., 2012). The rapid uptake of ^{70}Zn could be inferred from ^{70}Zn root concentration being around 70% of total Zn concentration (cf. Figure 2).

When natural isotopes are supplied in the nutrient culture, it is expected that the percentage of each isotope in the analysed plant tissue would follow its natural isotopic distribution, as confirmed for Zn isotopes in different wheat tissues (e.g. Wang et al., 2011). For example, relatively high proportions of ^{70}Zn were observed in wheat glumes (70%), peduncle (85%) and rachis (71-87% of the total Zn) (Wang et al. 2011), which is in accordance with the results of the present study (^{70}Zn was around 70% of the total Zn in radish roots, Figure 2).

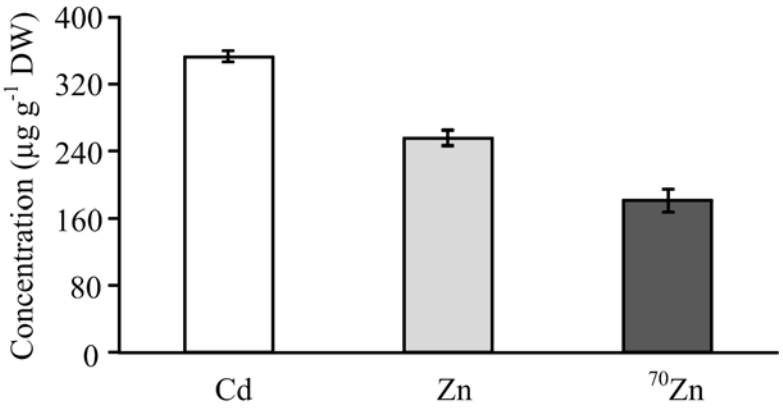

Figure 2. Concentration of total Cd, total Zn and ^{70}Zn in the bulk root tissue of radish (*Raphanus sativus* L. cv. Cherry Belle) after 24-hour exposure to the equimolar (2.2 μ*M*) Cd/^{70}Zn treatment. Error bars represent ±SE (n=3).

Cadmium was accumulated at higher (about 1.4-fold) concentration than Zn (Figure 2). Such result was in accordance with the recent study with 10 times longer (10 day) Cd exposure to twice higher (4.45 μ*M*) Cd concentration in radish root tissue (Ondrasek et al., 2018). Higher Cd than Zn concentration in root tissue (Figure 2) confirmed a strong capacity of radish roots to take up Cd (also in Ondrasek et al., 2018).

Cadmium and Zn are biogeochemically similar, mostly in the +2 oxidation state, but Cd has more complex chemistry in solution than Zn (Rehkämper et al., 2011). In most ecosystems, both trace metals occur predominantly in an ionic form as chlorides, nitrates, sulfates and phosphates (Wombacher and Rehkämper, 2004), and might be relatively easily available in the rhizosphere at suitable pHs. However, Cd ionic forms are likely to cross root and other bio-membranes via selective transporters/channels for similar essential nutrients (e.g. Zn, Fe, Ca) (Li et al., 2012) and/or via incompletely selective high/low affinity uptake systems (Wang et al., 2012). Also, from previous studies related to metals transport mostly in cereals (Herren and Feller, 1994; Pearson and Rengel, 1995; Rengel, 2001; Tauris et al., 2009; Wang et al., 2011) it was confirmed that Zn and some other divalent micronutrients (e.g. Mn, Fe) can be relatively easily and quickly taken up by roots and translocated by vascular components into other plant tissues. For instance, Zn was accumulated in the wheat crowns within an hour of exposure to ^{65}Zn (Pearson and Rengel, 1995).

Radish is widely cultivated crop grown in a range of agroecological conditions; generally, it can be considered a metal-sensitive species. For example, exposure to 4.45 μ*M* Cd contamination over a 10-day period induced tissue accumulation of Cd markedly above the

toxicity threshold (i.e. ~10 mg/kg on dry weight basis for Cd-sensitive species; Cabrera et al., 1988) causing shoot chlorosis and necrosis (Ondrasek et al., 2018). However, while radish roots showed relatively strong capacity to absorb Cd and Zn in the present study (Figure 2), their translocation to the edible hypocotyls and/or shoots was suppressed (Ondrasek et al., unpublished); similarly, after 10 days in 4.45 μ*M* Cd solution, the Cd tissue distribution was 51% in roots, 32% in shoots and 17% in hypocotyl (Ondrasek et al., 2018). In a different plant species, Lu et al. (2008) also noticed relatively low (less than 10% of total) root-to-shoot translocation of Cd in the non-hyperaccumulating vs. hyperaccumulating ecotypes of *Sedum alfredii*, probably as a consequence of enhanced xylem loading in the latter ecotype, as one of the important features of metal-tolerant plant species.

NanoSIMS maps of metal isotopes of interest in the apical root tissue

The successive sections of resin-embedded radish root apices were analysed by optical microscopy and NanoSIMS. Light microscopy of 1-μm-thick cross sections of root apices showed well-developed root cells (Figure 3a, b and c). Using the primary O^- ion beam (Figure 3d, e, f, g and h), the sections were scanned in the centripetal direction, i.e. from the edge (epidermal and outer cortical root layers) towards the centre (inner cortex layers and stele) of radish root apices; afterwards, the same areas were examined using the primary Cs^+ ion beam (Figure 3d, f and S1).

Even though both O^- and Cs^+ primary ion sources allowed mapping of the elemental distribution, the Cs^+ ion beam resulted in the elemental images of higher resolution than the O^- beam (Figure S1) due to a smaller beam diameter. In general, the distribution of Zn and Cd showed a decreasing trend from the outer root layer (epidermis - Ep) towards the centre (root endodermis - En and stele - S) (e.g. Figure 3e and h showed almost no Zn/Cd signal in the central area); in contrast, the distribution of other elements/complexes was relatively uniform across the scanned area (e.g. $^{35}Cl^-$, $^{32}S^-$, $^{26}CN^-$, Figure S1). This radial variability is important, given that

dynamics of transport into the central vascular elements from surrounding tissues might help de-couple root uptake from transport into, and utilization in, other plant tissues (Metzner et al., 2010), and contribute to elucidating elemental homeostasis at the (sub)cellular level (Bashir et al., 2016). Accordingly, the NanoSIMS approach applied here has advantages in tissue, cellular and subcellular elemental microanalyses due to high lateral resolution. In addition, imaging of the other highly diffusible ions such as Cl^- (Figure S1) confirmed that the sample preparation protocols and methods had not impacted their distribution, which is usually difficult to preserve; thus, we would suggest that the elemental distribution of other mobile isotopes of interest in the present study was also not altered. Importantly, freezing of plant specimens in liquid nitrogen for elemental analysis is a widely accepted technique, and while structural preservation may not be comparable to some other techniques (e.g. high-pressure freezing), the level of preservation is more than adequate for these types of analyses (e.g. McCully et al., 2010). Coupled with appropriate freeze-substitution techniques (e.g. use of non-polar solvents, anhydrous conditions, see Echlin, 1991), samples processed in this manner can be structurally well-preserved, with cellular ions retained and immobilised.

The previous studies revealed fast and heterogeneous (re)distribution of some elements within plant tissues in radial direction. For instance, in a tracer study performed on the frozen hydrated cross-sections of the bean stem employing the cryo-SIMS protocols, Metzner et al. (2010) detected fast (within minutes) and unhindered radial diffusivity of $H_2{}^{18}O$ as well as ^{26}Mg, ^{41}K and ^{44}Ca (all three nutrients exchanged large fractions, Ca even 100%, in-between the xylem vessels and surrounding parenchyma layers) across the examined area. In the study presented here, however, the trace element isotopes (^{70}Zn, ^{114}Cd) were virtually absent in the central (vascular) part of root apex after 24 h, confirming their slow transport from the root epidermis (Ep) across the cortical layer (Figure 3e and h). Substantially lower detection of ^{70}Zn (i.e. $^{70}Zn^+/^{64}Zn^+$ NanoSIMS ratio as HSI image) and ^{114}Cd in the root vascular region in comparison to the peripheral root area suggested relatively weak transport toward, and deposition/accumulation

356 in, other (older) root parts as well as edible hypocotyls and shoots, but further work is required for
357 confirmation.

358 Root tissues take up and transport water and nutrients in radial direction to the vascular
359 elements (e.g. xylem vessels) in the stele (Bramley et al., 2009; Persson et al., 2016) (Figure 1c,
360 d), thus contributing to nutrient transport into other tissues (Metzner et al., 2010). Radish root
361 apex represents a small portion of the root system (Figure 1a, b), but one of the fastest growing
362 plant tissues (with cellular divisions at the very tip and the cellular elongation in more proximal
363 cells) and very propulsive region for elements fluxes. For instance, employing the ion-selective
364 electrode technique to investigate the cadmium fluxes in different root apex regions of halophyte
365 plant species *Sueada salsa*, Li et al. (2012) detected that Cd^{2+} influx was the greatest within 150
366 μm of the root tip after high Cd contamination (100 μM) during 24-h exposure. Interestingly, at
367 the position beyond 20 mm from the root apex, there were no measurable Cd^{2+} fluxes.

368 The two elements of interest in the study presented here are either required by cells in
369 relatively small amounts (Zn) or not at all (Cd, but its uptake cannot be avoided). It was shown
370 that Cd (and some other trace metals such as Pb, Cu, Ti) can induce positive, i.e. stimulating
371 phyto-reactions (e.g. increased growth, chlorophyll/protein content, photosynthetic activity, dry
372 weight), but at ultra-trace concentrations (Appenroth, 2010; Kovács-Bogdán et al., 2010) applied
373 to the rhizosphere or foliage. Some of these positive responses (i.e. increase in photosynthetic
374 activity/CO_2 fixation and/or chlorophyll content) to Cd exposure as a low-dose phyto-stressor
375 were confirmed in the hydroponically-treated maize and barley seedlings (at concentration 44-
376 fold lower (0.05 μ*M* Cd) than in the study presented here) (Nytrai et al. 2003) and sprayed bean
377 seedlings (at concentration 4.4-fold lower (0.5 μ*M* Cd) than in the study presented here) (Kovács
378 et al. 2009).

379 Plant uptake and inter-tissue transport/accumulation of Cd (and other trace elements) is
380 markedly governed by the conditions in the rhizosphere, xylem/phloem sap, cytosol, etc.,
381 including pH, element concentration/activity, presence of in/organic complexing agents, redox

potential, etc. (e.g. Ondrasek, 2013; Augustynowicz et al., 2014). An excellent example is chromium (Cr) with different oxidation states; Cr(III) as essential microelement for mammals (but no clear function in plants) and toxic Cr(VI) resulted in significant differences in Cr uptake and distribution in macrophyte *Callitriche cophocarpa* (Augustynowicz et al., 2014). Chromium (III) was exclusively deposited in epidermal glands/hairs, whereas hexavalent Cr was detected predominantly in the vascular bundles of *C. cophocarpa* shoots (Augustynowicz et al., 2014). Similarly in the case of physicochemical similarity between Cd and Zn, it is unavoidable for Cd to be taken up and translocated within plants using Zn pathways (Figure 3).

It is likely that older root tissues would accumulate Zn and Cd to a greater extent than the young meristematic tissues, particularly because mature endodermis (in its tertiary state of development, i.e. comprising also suberin lamellae and thickened cell walls; Bramley et al., 2009; Persson et al., 2016) in such older tissues would contain less-permeable Casparian strip impacting negatively the transfer of trace metals to the stele and long-distance transport to other plant tissues, thus keeping an increasing proportion of ions in the root tissue external to, and including, endodermis. Contributing to this hypothesis, Ma and Yamaji (2008) reported that silicon transporters (Lsi1 and Lsi2) (responsible for Si transport in rice from the external solution to the root and further across the cortex to the stele) are localized in the root zones where Casparian strip developed. In addition, the expression of *Lsi1* and accumulation of *Lsi2* transcripts were lower in the root apex region (up to 10 mm from the tip, as used in this study; Figure 1b, c), than in the older regions (>10 mm from the tip) (Yamaji and Ma, 2007; Ma et al., 2007). In line with this suggestion, Sparks et al. (2011) employed the SIMS analyses on the monocot grass root tissues to localise Si and Ge mostly in the suberized thick-walled region of endodermal cells with well-developed Casparian strip. Thus, bioimaging of trace element isotopes of Cd and Zn by NanoSIMS is expected to be highly challenging in the meristematic root zone with immature endodermis and still developing Casparian strip (Figure 1a, b) vs. mature root zones, emphasising the importance of findings reported in the present study.

408

409

410

Figure 3. Serial cross-section images of radish (*Raphanus sativus* L. cv. Cherry Belle) apical root tissue exposed to the equimolar (2.2 μ*M*) Cd/^{70}Zn treatment for 24 h. All NanoSIMS images are 50 μm x 50 μm. The black and white arrows show centripetal direction of NanoSIMS scanning, i.e. from the root epidermis (Ep), exodermis (Ex), cortex (Co) and endodermis (En) towards the centre of the root apex or stele (S).

(a, b and c) Optical micrographs of resin-embedded cross sections of radish apical root tissue prepared by freezing in liquid nitrogen followed by freeze substitution. Red squares represent the regions of interest scanned by NanoSIMS.

(d, e, f, g and h) NanoSIMS images obtained using the O^- primary ion beam for the distribution of $^{64}Zn^+$, $^{70}Zn^+$ and $^{114}Cd^+$ signals from the regions of interest. The secondary electron (SE) images acquired with the Cs^+ beam are included to show the surface morphology of the imaged region. The $^{70}Zn^+/^{64}Zn^+$ NanoSIMS ratio images are shown as hue saturation intensity (HSI images) of the region of interest confirming ^{70}Zn enrichment in some parts of root cells. In HSI images, the colour scale indicates the $^{70}Zn^+/^{64}Zn^+$ ratio, with the natural abundance levels (blue, 127) changing to pink (1000) with increasing ^{70}Zn proportion.

Different genotypes of a given species may exhibit significant differences in metal elements acquisition, root-to-shoot transport and/or accumulation. For instance, *Sedum alfredii* as a native Cd/Zn hyperaccumulator has different ecotypes that express contrasting physiological responses depending on metal contamination. Lu et al. (2008) noticed that Cd root influx in both *Sedum alfredii* ecotypes (NHE - non-hyperaccumulating and HE - hyperaccumulating) was carrier-mediated, but apoplastic Cd binding was significantly higher in the NHE ecotype. Also, the NHE (*vs.* HE) ecotype had 2-fold lower Cd symplastic uptake rate as well as enhanced Cd root sequestration accompanied by reduced Cd xylem transport rate and 3-5 times lower Cd concentration in the xylem sap. Moreover, Lu et al. (2008) noticed that after the Cd treatment

436 (100 μM for 6-24 h), the HE ecotype preferentially localised Cd in the root central cylinder (stele)
437 in contrast to the NHE ecotype whose Cd localisation was relatively uniform across the whole
438 root (but the resolution of the technique used was not sufficient to assess the Cd distribution at the
439 sub-cellular scale). Similar observation regarding Cd localisation in the vascular apical root tissue
440 was recorded by Li et al. (2012) in halophyte *Suaeda salsa* after root exposure to 100 μM
441 $Cd(NO_3)_2$ for 24 h. However, in our study, Cd (Zn) root localisation was quite different to those
442 in the HE *Sedum alfredii* ecotype (Lu et al. 2008) and halophyte *Suaeda salsa* (Li et al. 2012),
443 suggesting different uptake/transport routes of Cd (Zn) in metal- or salt-tolerant species and
444 metal-sensitive plant species (such as radish used in the present study).

445 In this study, it was relatively difficult to determine precisely the elemental distribution
446 intracellularly. However, considering both primary ion sources used, the highest accumulation of
447 Zn and Cd was detected at the cell periphery (Figure 3d and f), corresponding to the cell wall
448 structures whose negative charges (arising from the presence of carboxyl, sulfhydryl, hydroxyl
449 and amino/aldehyde groups) serve as the first barrier protecting the protoplasts from metal ion
450 toxicity (e.g. Wang et al., 2011; Augustynowicz et al., 2014). Similarly, apoplastic Cd binding
451 was significantly higher in the NHE than the HE *Sedum alfredii* ecotype (Lu et al. 2008), and Cd
452 was stored predominantly in the cell wall fraction of apple (metal-sensitive) rootstock (Zhou et al.
453 2017).

454 NanoSIMS has sufficient spatial resolution and analytical sensitivity to be a successful
455 technique for elemental mapping at the subcellular level, as shown in case of Se and As in rice
456 grains (Moore et al., 2010) or Ni, P and S in the leaf trichomes of *Alyssum lesbiacum* (Smart et
457 al., 2010). However, successful subcellular elemental imaging by NanoSIMS is affected by the
458 method of sample preparation employed (whether optimised for structural preservation or
459 retention of cellular ions, which typically require different approaches), is dependent on specimen
460 topography (emphasising a need for flat sections) and is subject to strong matrix effects (Smart et

al., 2010) (e.g. elemental signals from a different matrix types such as vacuole or nucleus vs. cytoplasm affect map quality of a particular element).

CONCLUSIONS

Metal-sensitive radish (17-d-old) exposed to relatively low Zn and Cd contamination for 24 h showed strong accumulation of these metal ions in the root, suggesting relatively poor and slow translocation of Zn and Cd to shoots. Using NanoSIMS, we mapped the accumulation of ^{70}Zn and ^{114}Cd in various root apical tissues *in situ* for the first time. Accumulation of Zn and Cd isotopes decreased markedly from the epidermis through to the cortex and the stele, suggesting that the observed elements share similar transport pathways in the root cells and tissues.

NanoSIMS had sufficient spatial resolution and analytical sensitivity to map the distribution of a range of elements and functional groups/molecules in root cells. However, localisation and imaging of Cd and Zn isotopes at the subcellular level remains technically-challenging, especially at sub-toxic concentrations and short-term exposure.

ACKNOWLEDGMENTS

The authors acknowledge the facilities and scientific and technical assistance of the Australian Microscopy and Microanalysis Research Facility at the Centre for Microscopy, Characterisation and Analysis, University of Western Australia, a facility funded by the university and state and Commonwealth governments. Also, we are grateful to anonymous reviewers for the valuable comments and suggestions that helped improve the manuscript. This research has been provided under the Research Executive Agency of the European Union grant number FP7 MC-IOF 330669.

References

Adriano, D.C., Wenzel, W.W., Vangronsveld, J., and Bolan, N.S., 2004. Role of assisted natural remediation in environmental cleanup. Geoderma 122, 121-142.

Appenroth, KJ. Acta Physiol Plant (2010) 32: 615. https://doi.org/10.1007/s11738-009-0455-4

Augustynowicz J, Wróbel P, Płachno BJ, Tylko G, Gajewski Z, Węgrzynek D., 2014. Chromium distribution in shoots of macrophyte *Callitriche cophocarpa* Sendtn. Planta 239, 1232–1242. doi: 10.1007/s00425-014-2047-9.

Bashir, K., Rasheed, S, Kobayashi, T., Seki, M and Nishizawa, N.K., 2016. Regulating Subcellular Metal Homeostasis: The Key to Crop Improvement. Front. Plant Sci. **7**:1192. doi: 10.3389/fpls.2016.01192.

Boxer, S.G., Kraft, M.L., and Weber, P.K., 2009. Advances in Imaging Secondary Ion Mass Spectrometry for Biological Samples. Annu. Rev. Biophys. 38, 53-74.

Bramley, H., Turner, N.C., Turner, D.W., and Tyerman, S.D., 2009. Roles of morphology, anatomy, and aquaporins in determining contrasting hydraulic behavior of roots. Plant Physiol. 150(1), 348-364.

Broadley, M.R., White, P.J., Hammond, J.P., Zelko, I., and Lux, A., 2007. Zinc in plants. New Phytol. 173, 677-702.

Buffet P.E., Amiard-Triquet C, Dybowska A, Risso-de Faverney C, Guibbolini M, Valsami-Jones E, Mouneyrac C. 2012. Fate of isotopically labeled zinc oxide nanoparticles in sediment and effects on two endobenthic species, the clam *Scrobicularia plana* and the ragworm *Hediste diversicolor*, Ecotoxicology and Environmental Safety (84), 191-198, doi.org/10.1016/j.ecoenv.2012.07.010.

508 Cabrera, D., Young, S.D., Rowell, D.L., 1988. The toxicity of cadmium to barley plants as
509 affected by complex formation with humic acid. Plant Soil 105, 195–204.

510 Chandra, S., 2008. Challenges of biological sample preparation for SIMS imaging of elements
511 and molecules at subcellular resolution. Appl. Surf. Sci. 255(4), 1273-1284.

512 Cennerazzo, J., de Junet, A., Audinot, J.N., Leyval, C., 2017. Dynamics of PAHs and derived
513 organic compounds in a soil-plant mesocosm spiked with ^{13}C-phenanthrene. Chemosphere 168,
514 1619-1627.

515 Clemens, S., 2006. Toxic metal accumulation, responses to exposure and mechanisms of
516 tolerance in plants. Biochimie 88, 1707-1719.

517 Clode, P.L., Kilburn, M.R., Jones, D.L., Stockdale, E.A., Cliff, J.B., Herrmann, A.M., and
518 Murphy, D.V., 2009. In situ mapping of nutrient uptake in the rhizosphere using nanoscale
519 secondary ion mass spectrometry. Plant Physiol. 151, 1751-1757.

520 Das, P., Samantaray, S., and Rout, G.R., 1997. Studies on cadmium toxicity in plants: A review.
521 Environ Pollution. 98, 29-36.

522 Echlin, P., 1991. Low temperature microscopy and analysis. Plenum Press, New York.

523 Eybe, T., Audinot, J.N., Udelhoven, T., Lentzen, E., El Adib, B., Ziebel, J., Hoffmann, L., Bohn,
524 T., 2013. Determination of oral uptake and biodistribution of platinum and chromium by the
525 garden snail (*Helix aspersa*) employing nano-secondary ion mass-spectrometry, Chemosphere
526 90(6), 1829-1838.

527 Eybe, T., Bohn, T., Audinot,J.N., Udelhoven, T., Cauchie,H.M., Migeon, H.N., Hoffmann, L.,
528 2009. Uptake visualization of deltamethrin by NanoSIMS and acute toxicity to the water flea
529 *Daphnia magna*. Chemosphere 76(1), 134-140.

530 Hart, J.J., Welch, R.M., Norvell, W.A., Kochian, L.V., 2002. Transport interactions between
531 cadmium and zinc in roots of bread and durum wheat seedlings. Physiol Plant. 116, 73-78.

532 Hart, J.J., Welch, R.M., Norvell, W.A., Sullivan, L.A., Kochian, L.V., 1998. Characterization of
533 cadmium binding, uptake, and translocation in intact seedlings of bread and durum wheat
534 cultivars. Plant Physiol. 116, 1413-1420.

535 Herren, T., and Feller, U., 1994. Transfer of zinc from xylem to phloem in the peduncle of wheat.
536 J. Plant Nutr. 17, 1587-1589.

537 Huang, Y., He, C., Shen, C., Guo, J., Mubeen, S., Yuan, J., and Yang, Z., 2017. Toxicity of
538 cadmium and its health risks from leafy vegetable consumption. Food Funct. 8(4), 1373-1401.

539 Kilburn, M.R., Clode P.L., 2014. Elemental and isotopic imaging of biological samples using
540 NanoSIMS. In: Kuo J. (eds) Electron Microscopy. Methods in Molecular Biology (Methods and
541 Protocols), vol 1117. Humana Press, Totowa, NJ.

542 Kilburn, M.R., Jones, D.L., Clode, P.L., Cliff, J.B., Stockdale, E.A., Herrmann, A.M., Murphy,
543 D.V., 2010. Application of nanoscale secondary ion mass spectrometry to plant cell research.
544 Plant Signaling Behav. 5(6), 760-762.

545 Kovács E, Nyitrai P, Czövek P, Óvári M, Keresztes Á., 2009. Investigation into the mechanism of
546 stimulation by low-concentration stressors in barley seedlings. J. Plant Phys. 166, 72-79.

547 Erika Kovács-Bogdán, Péter Nyitrai & Áron Keresztes. 2010. How does a little stress stimulate a
548 plant?, Plant Signaling & Behavior, 5(4), 354-358, DOI: 10.4161/psb.5.4.10870

549 Li L, Liu X, Peijnenburg W.J.G.M., Zhao J, Chen X, Yu J, Wu H. 2012. Pathways of cadmium
550 fluxes in the root of the halophyte *Suaeda salsa*, Ecotoxicology and Environmental Safety, (75):1-
551 7, doi.org/10.1016/j.ecoenv.2011.09.007.

552 Lombi, E., Scheckel, K.G., and Kempson, I.M., 2011. In situ analysis of metal(loid)s in plants:
553 state of the art and artefacts. Environ Exp Bot. 72, 3-17.

554 Lu, L.L., Tian, S.K., Yang, X.E., Wang, X.C., Brown, P., Li, T.Q., He, Z.L., 2008. Enhanced
555 root-to-shoot translocation of cadmium in the hyperaccumulating ecotype of *Sedum alfredii*. J.
556 Exp. Bot. 59, 3203–3213.

557 Ma, J.F., Yamaji, N., 2008. Functions and transport of silicon in plants. Cell Mol. Life Sci.
558 65(19), 3049-3057.

559 Ma, J.F., Yamaji, N., Mitani, N., Tamai, K., Konishi, S., Fujiwara, T., Katsuhara, M. and Yano,
560 M. (2007). An efflux transporter of silicon in rice. Nature 448, 209-211.

561 Marschner, P., 2012. Marschner's Mineral Nutrition of Higher Plants, Academic Press.

562 McCully, M., Canny, M., Huang, C., Miller, C., Brink, F., 2010. Cryo-scanning electron
563 microscopy (CSEM) in the advancement of functional plant biology: energy dispersive X-ray
564 microanalysis (CEDX) applications. Funct. Plant Biol. 37, 1011–1040.

565 Metzner, R., Thorpe, M.R., Breuer, U., Blümler, P., Schurr, U., Schneider, H.U., Schroeder,
566 W.H., 2010. Contrasting dynamics of water and mineral nutrients in stems shown by stable
567 isotope tracers and cryo-SIMS. Plant Cell Environ. 33, 1393-1407.

568 Moore, K.L., Chen, Y., van de Meene, A.M.L., Hughes, L., Liu, W., Geraki, T., Mosselmans, F.,
569 Mcgrath, S.P., Grovenor, C., and Zhao, F.J., 2014. Combined NanoSIMS and synchrotron X-ray
570 fluorescence reveals distinct cellular and subcellular distribution patterns of trace elements in rice
571 tissues. New Phytol. 201(1), 104-115.

572 Moore, K.L., Lombi, E., Zhao, F.J., and Grovenor, C.R.M., 2012. Elemental imaging at the
573 nanoscale: NanoSIMS and complementary techniques for element localisation in plants. Anal.
574 Bioanal. Chem. 402, 3263–3273.

575 Moore, K.L., Schroder, M., Wu, Z., Martin, B., Hawes, C., McGrath, S.P., Hawkesford, M.J., Ma,
576 J.F., Zhao, F.J., and Grovenor, C.R.M., 2011. High resolution secondary ion mass spectrometry
577 reveals the contrasting subcellular distribution of arsenic and silicon in rice roots. Plant Physiol.
578 156, 913-924.

579 Moore KL, Schroder M, Lombi E, Zhao FJ, McGrath SP, Hawkesford MJ, Shewry PR, Grovenor
580 C.R.M., 2010. NanoSIMS analysis of arsenic and selenium in cereal grain. New Phytol. 185, 434-
581 445.

582 Nakanishi, H., Ogawa, I., Ishimaru, Y., Mori, S., Nishizawa, N.K., 2006. Iron deficiency
583 enhances cadmium uptake and translocation mediated by the Fe^{2+} transporters OsIRT1 and
584 OsIRT2 in rice. Soil. Sci. Plant. Nutr. 52, 464-469.

585 Nyitrai P, Bóka K, Gáspár L, Sárvári É, Lenti K, Keresztes Á., 2003. Characterisation of the
586 stimulating effect of low-dose stressors in maize and bean seedlings. J. Plant Physiol. 160, 1175-
587 1183.

588 Ondrasek, G., Rengel, Z., Romic, D., 2018. Humic acids decrease uptake and distribution of trace
589 metals, but not the growth of radish exposed to cadmium toxicity. Ecotox. Environ. Safe. 151(30),
590 55-61.

591 Ondrasek, G., 2013. The responses of salt-affected plants to cadmium, in Salt Stress in Plants:
592 Signalling, Omics and Adaptations, eds. Ahmad P., Azooz M.M., Prasad M.N.V. (New York,
593 Springer), p. 439-463.

594 Ondrasek, G., Rengel, Z., Romic, D., Savic, R., 2012. Salinity decreases dissolved organic carbon
595 in the rhizosphere and increases trace elements phyto-accumulation. Eur. J. Soil. Sci. 63(5), 685-
596 693.

597 Pearson, J.N., Rengel, Z., Graham, R.D., 1999. Regulation of zinc and manganese transport into
598 developing wheat grains having different zinc and manganese concentrations. J. Plant. Nutr. 22,
599 1141-1152.

600 Pearson, J.N., Rengel, Z., 1995. Uptake and distribution of ^{65}Zn and ^{54}Mn in wheat grown at
601 sufficient and deficient levels of Zn and Mn. I. During vegetative growth. J. Exp. Bot. 46(288),
602 833-839.

603 Pérez-López, M., Hermoso de Mendoza, M., López Beceiro, A., Soler Rodríguez, F. 2008. Heavy
604 metal (Cd, Pb, Zn) and metalloid (As) content in raptor species from Galicia (NW Spain),
605 Ecotoxicology and Environmental Safety, Volume 70, Issue 1, 2008, Pages 154-162,
606 https://doi.org/10.1016/j.ecoenv.2007.04.016.

607 Persson, D.P., Chen, A., Aarts, M.G.M., Salt, D.E., Schjoerring, J.K., Husted, S., 2016. Multi-
608 element bioimaging of *Arabidopsis thaliana* roots. Plant. Physiol. 172(2), 835-847.

609 Rehkämper, M., Wombacher, F., Horner, T.J., Xue, Z., 2011. Natural and anthropogenic Cd
610 isotope variations, in Handbook of Environmental Isotope Geochemistry, Advances in Isotope
611 Geochemistry, ed. M. Baskaran, Springer-Verlag, Berlin Heidelberg, 125-154.

612 Rengel, Z., 2015. Availability of Mn, Zn and Fe in the rhizosphere. J. Soil. Sci. Plant. Nutr. 15(2),
613 397-409.

614 Rengel, Z., 2001. Xylem and phloem transport of micronutrients, in Plant Nutrition – Food
615 Security and Sustainability of Agroecosystems, eds. Horst WJ et al. (Dordrecht, the Netherlands,
616 Kluwer Academic Publishers), pp. 628-629.

617 Salt, D.E., Prince, R.C., Pickering, I.J., Raskin, I., 1995. Mechanisms of cadmium mobility and
618 accumulation in Indian mustard. Plant Physiol. 109, 1427-1433.

619 Savic, R., Ondrasek, G., Josimov-Dundjerski, J., 2014. Heavy metals in agricultural landscapes as
620 hazards to human and ecosystem health: A case study on zinc and cadmium in drainage channel
621 sediments. J. Sci. Food. Agric. 95(3), 466-470.

622 Sigel, A., Sigel, H., and Sigel, R.K.O., 2013. Cadmium: From Toxicity to Essentiality. Springer,
623 Dordrecht.

624 Smart, K.E., Smith, J.A.C., Kilburn, M.R., Martin, B.G.H., Hawes, C., Grovenor, C.R.M., 2010.
625 High-resolution elemental localization in vacuolate plant cells by nanoscale secondary ion mass
626 spectrometry. Plant J. 63, 870-879.

627 Smart, K.E., Kilburn, M.R., Salter, C.J., Smith, J.A.C., Grovenor, C.R.M., 2007. NanoSIMS and
628 EPMA analysis of nickel localisation in leaves of the hyperaccumulator plant *Alyssum lesbiacum*.
629 Int. J. Mass. Spec. 260, 107-14.

630 Sparks, J.P., Chandra, S., Derry, L.A., Parthasarathy, M.V., Daugherty, C.S., Griffin, R., 2011.
631 Subcellular localization of silicon and germanium in grass root and leaf tissues by SIMS:
632 evidence for differential and active transport. Biogeochem. 104, 237-249.

633 Tartivel, R., Tatin, R., Delhaye, T., Maupas, A., Gendron, A., Gautier, S., Lavastre, O., 2012.
634 Visualization and localization of bromotoluene distribution in *Hedera helix* using NanoSIMS.
635 Chemosphere 89(7), 805-809.

636 Tauris, B., Borg, S., Gregersen, P.L., Holm, P.B., 2009. A roadmap for zinc trafficking in the
637 developing barley grain based on laser capture microdissection and gene expression profiling. J.
638 Exp. Bot. 60, 1333-1347.

639 Villafort Carvalho, M.T., Pongrac, P., Mumm, R., van Arkel, J., van Aelst, A., Jeromel, L.,
640 Vavpetič, P., Pelicon, P., Aarts, M.G.M., 2015. *Gomphrena claussenii*, a novel metal-
641 hypertolerant bioindicator species, sequesters cadmium, but not zinc, in vacuolar oxalate crystals.
642 New Phytol. 208(3), 763-775.

643 Wang, Y.X., Specht, A., Horst, W.J., 2011. Stable isotope labelling and zinc distribution in grains
644 studied by laser ablation ICP-MS in an ear culture system reveals zinc transport barriers during
645 grain filling in wheat. New Phytol. 189(2), 428-437.

646 Wang M, Chen Li, Chen S, Ma Y. 2012. Alleviation of cadmium-induced root growth inhibition
647 in crop seedlings by nanoparticles, Ecotoxicology and Environmental Safety, 79(48-54).
648 doi.org/10.1016/j.ecoenv.2011.11.044.

649 Wombacher, F., Rehkämper, M., 2004. Problems and suggestions concerning the notation of
650 cadmium stable isotope compositions and the use of reference materials. Geostand. Geoanal. Res.
651 28, 173-178.

652 Yamaji, N. and Ma, J.F., 2007. Spatial distribution and temporal variation of the rice silicon
653 transporter Lsi1. Plant Physiol. 143, 1306-1313.

654 Zhou, J., Wan, H., He, J., Lyu, D., Li, H., 2017. Integration of cadmium accumulation, subcellular
655 distribution, and physiological responses to understand cadmium tolerance in apple rootstocks.
656 Front. Plant. Sci. 8, 966. doi: 10.3389/fpls.2017.00966.

657

658

659

660

661

662

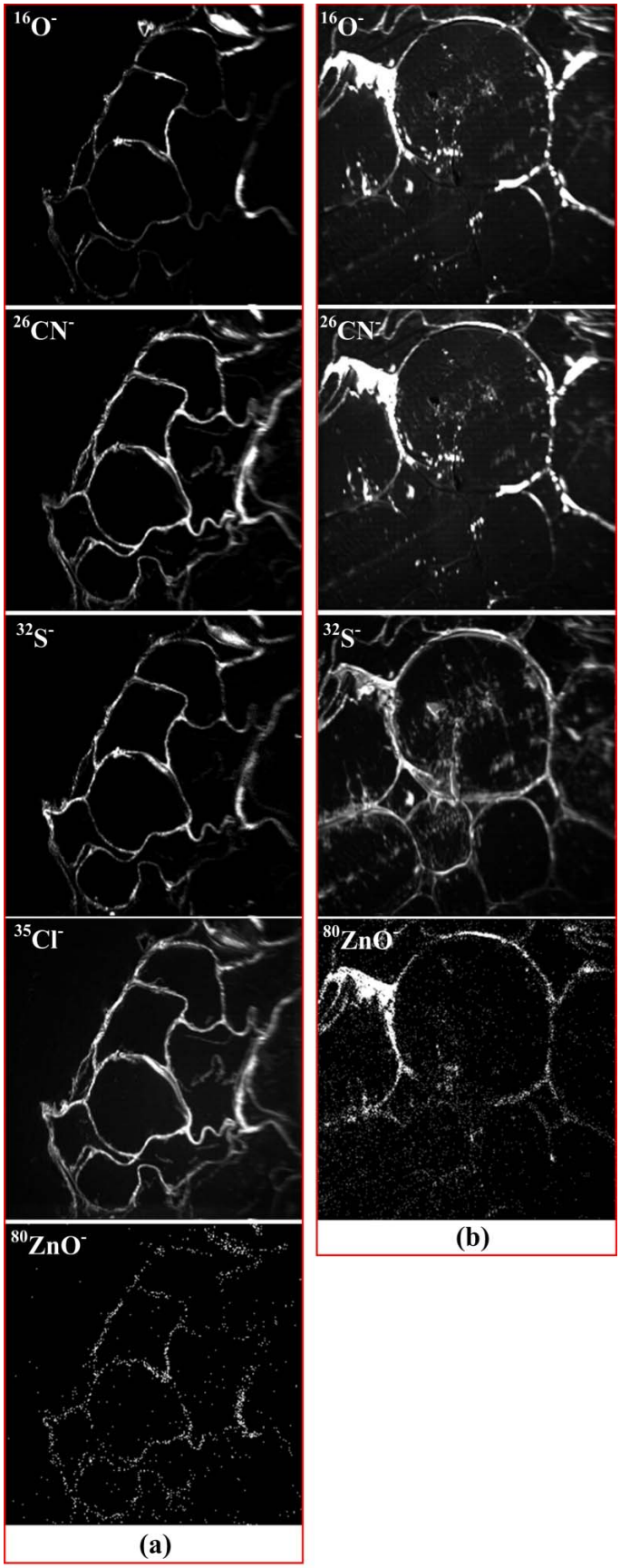

Figure S1. NanoSIMS images obtained using the Cs^+ primary ion beam to show the distribution of $^{16}O^-$, $^{26}CN^-$, $^{32}S^-$, $^{35}Cl^-$ and $^{80}ZnO^-$ signals from the region of interest (a=section 1 and b=section 2).